# Molecular Dynamics Simulation of the LOV2 Domain from *Adiantum capillus-veneris*

Christian Neiss*,† and Peter Saalfrank‡

Institut für Physikalische und Theoretische Chemie, Universität Regensburg, Universitätsstrasse 31, D-93053 Regensburg, Germany, and Institut für Chemie, Universität Potsdam, Karl-Liebknecht-Strasse 24-25, D-14476 Potsdam-Golm, Germany

Received April 5, 2004

The mechanism for signal transduction from the LOV-domains toward the kinase region of phototropin is still not well understood. We have performed molecular dynamics (MD) simulations and CONCOORD calculations on the LOV2 domain of *Adiantum capillus-veneris*, with the goal to detect possible differences between the two forms of the LOV domain which may not show up in the static crystal structures. Since no such clear differences are found in the MD simulations also, we suggest that the real, biologically active conformation of the LOV domain within the whole phototropin is different from the crystal structure of the isolated LOV domains. The MD simulations do offer, however, insight into details of the dynamics of the dark and illuminated LOV domains, which are discussed in the light of recent experiments.

## 1. INTRODUCTION

Intense experimental and theoretical work on phototropins has established a highly active subfield of research on biologically active photoreceptors during the past few years—see ref 1 or a recent review. It is known that phototropins not only mediate phototropism in plants[2,3] but also various other photoresponses such as chloroplast relocation,[4,5] the opening of guard cells,[6] and gametogenesis (in *Chlamydomonas reinhardtii*).[7,8] The principal structure of these proteins contains three important subdomains, namely two so-called LOV domains (LOV1 and LOV2), each of them containing one chromophore molecule FMN and a Ser/Thr kinase region. The latter has been found to be multiple phosphorylated upon blue-light illumination of the protein.[2,3] However, not both LOV domains are necessary for activating the kinase. Christie et al. have shown in the case of *Arabidopsis thaliana* that LOV1 can be deactivated without detectable loss of autophosphorylation of the kinase, whereas a functioning LOV2 domain is crucial.[9] Therefore, the two LOV domains seem to have different functions/importance. In fact, the role of the LOV1 domain remains largely unclear, but it is conjectured that it might be the more important domain for protein−protein dimerization.[9] The LOV domains belong to the PAS domain super family, whose members are known to mediate protein−protein interactions. Therefore, one may speculate that LOV domains share this function, however, via a light-induced mechanism. Again, the partner of phototropin for such a dimerization is still not known.

The initial photoreaction within the LOV domains has been studied in quite some detail by various experimental[10−12] and theoretical means.[13] In brief, the mechanism is as follows. After photoexcitation from the ground to an excited singlet state, FMN relaxes by internal conversion and intersystem crossing to the lowest triplet state, $T_1$, on the time scale of a few nanoseconds. Within microseconds the triplet state then reacts intramolecularly to a covalent adduct configuration with a nearby cysteine residue, i.e., an S−H-bond is being broken and N−H and C−S bonds are being formed.[14,11,15] The adduct form then reacts thermally back to the initial, dark state within a few minutes. From there, the cycle can start again.

These findings are also supported by crystal structures of the illuminated state, taken from singly expressed LOV domains.[16−18] The crystal structures revealed no significant conformational changes of the LOV domains upon adduct formation, relative to the dark state. This comes as a surprise because the signal has to be transported to the kinase region somehow, and conformational changes in the LOV domain are one possible route along which this may happen. There are at least two possible explanations for this finding: First, one or both of the dark and the illuminated state(s) do(es) not reflect the structure of the LOV domain in the entire, biologically active phototropin and/or parts of the system essential for the signaling are missing in the crystal structure. Second, it may also be that the signal is not transported by a conformation change that leaves its traces in the static crystal structure but rather by, e.g., the different mobility of certain parts of the LOV domain, i.e. by *dynamics*. This second possibility has been discussed by Crosson et al.[1] Based on their crystal structures and similar findings for PYP (photoactive yellow protein), they claim that a conserved salt bridge on the surface of the LOV domain opens or at least becomes more flexible in the illuminated (adduct) state.

In this paper we will investigate this possibility theoretically. To do so, and also to get a deeper insight into the differences between the dark and the signaling state of the LOV domains in general, we performed molecular dynamics (MD) simulations for both states of the LOV2 domain of *Adiantum capillus-veneris*. These results were, partially, compared to results obtained with the program CONCOORD.[19] The latter allows for a very efficient generation of a

* Corresponding author phone: +49 (7247) 82-6380; fax: +49 (7247) 82-6368; e-mail: christian.neiss@int.fzk.de. Present address: Institut f. Nanotechnologie, Forschungszentrum Karlsruhe, Hermann-von-Helmholtz-Platz 1, D-76344 Eggenstein-Leopoldshafen, Germany.

† Universität Regensburg.

‡ Universität Potsdam.

10.1021/ci049883u CCC: $27.50 
Published on Web 08/07/2004

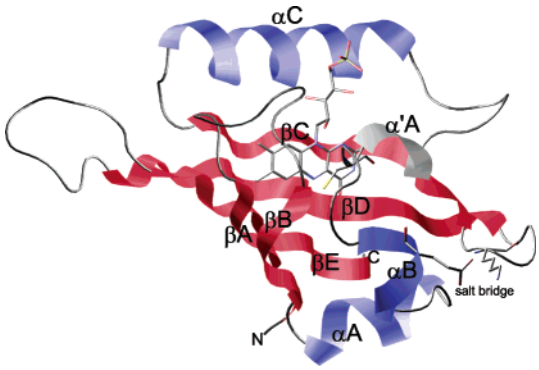


**Figure 1.** Crystal structure of the dark state of the LOV2 domain from *Adiantum capillus-veneris* (pdb code: 1G28). Note the flavin unit in the center and the cysteine (Cys38) unit close to it. Also indicated is the salt bridge (Glu32-Lys73). Red atoms: oxygen; blue: nitrogen, yellow: sulfur. Generated with VMD.[23]

large number of possible molecular configurations, by bypassing costly MD simulations.

Some details of the MD and the CONCOORD simulations will be outlined in the next two subsections 2.1 and 2.2. In section 3 our results will be presented and discussed, while section 4 summarizes this work.

## 2. COMPUTATIONAL METHODS

**2.1. Molecular Dynamics Simulations.** The program package GROMACS 3.1.4,[20,21] together with the GROMOS96 (version 43a1) force field[22] was used for the MD simulations. As starting geometries the crystal structures of the dark and the illuminated (adduct) form of the LOV2 domain of *Adiantum capillus-veneris* were used (pdb codes 1G28 and 1JNU, respectively).[16,17] Altogether, there are 104 amino acids in the LOV2 domain. For clarity, the crystal structure of the dark form is shown in Figure 1.

Side chains which were missing in the pdb files were added in "extended" conformation. Also hydrogen atoms were added, whereby basic side chains were protonated and acidic ones were left deprotonated, yielding a total charge of $-2e$ for the LOV domains. Aliphatic hydrogens are treated in an united atom approach, together with the carbon atom they are attached to.

For the adduct form a new amino acid, namely "cysteinyl-FMN" consisting of 44 atoms, had to be parametrized for the force field. This was done by using the predefined GROMOS atom types. The parametrization, along with a pictorial representation of "cysteinyl-FMN" are given in the Supporting Information.

Each of the two proteins was centered in a periodic, rhombic dodecahedral simulation box with a minimum protein-box distance of 1.0 nm. The resulting box volumes for the dark and the signaling state are 224.08 $nm^3$ and 227.79 $nm^3$, respectively. The boxes were filled with 6883 and 6954 SPC water molecules[24] for the dark and illuminated forms, respectively.

Two $Na^+$ cations were added in each case to ensure charge neutrality of the simulation cells.

To relax the configuration of the solvent and of the added amino acid side chains, a steepest descent minimization was adopted. During this procedure those atoms which could be resolved in the crystal structures were position-restrained at their initial positions by application of a harmonic potential with a large force constant of 25000 kJ $mol^{-1}$ $nm^{-2}$.

**Table 1.** Equilibration Protocol of the MD Simulations

| step | duration [ps] | $T_0$ [K] | $\tau_T$ [ps] | $k_{pr}$ [kJ $mol^{-1}$ $nm^{-2}$] | ensemble | $\tau_p$ [ps] |
|---|---|---|---|---|---|---|
| 1 | 5 | 50 | 0.1 | 25000 | NVT | |
| 2 | 5 | 100 | 0.01 | 10000 | NVT | |
| 3 | 5 | 150 | 0.01 | 5000 | NVT | |
| 4 | 5 | 200 | 0.01 | 1000 | NVT | |
| 5 | 5 | 250 | 0.01 | 100 | NVT | |
| 6 | 5 | 300 | 0.01 | 10 | NVT | |
| 7 | 5 | 300 | 0.1 | 0 | NPT | 1.0 |

The geometry-optimized structures were then heated stepwise, to a finite temperature of 300 K. This was done by using the Berendsen coupling to a bath with temperature $T_0$[25] and a relaxation time $\tau_T$:

$$\frac{dT(t)}{dt} = \frac{T_0 - T(t)}{\tau_T} \quad (1)$$

The time step used in all calculations was 1.0 fs. Initial velocities were randomly generated from a Maxwell distribution at 50 K. To control the quality of the sampling in our simulations, for each form two different velocity distributions were generated initially, resulting in two simulations each for the dark and the adduct (illuminated, signaling) state, respectively.

The water plus $Na^+$ ion subsystem was coupled separately from the protein to the temperature bath to avoid artificial heating of the former. During equilibration, the protein and FMN atoms (except hydrogens) were position-restrained by applying a harmonic interaction starting with a force constant of 25000 kJ $mol^{-1}$ $nm^{-2}$ in the first step. Details of the equilibration protocol are shown in Table 1. During the last step of equilibration also a weak pressure coupling was adopted, with a relaxation time $\tau_p$.[25]

Bond distances were kept fixed using the SETTLE algorithm[26] for SPC water and the LINCS algorithm[27] for all other bonds. van der Waals interactions were computed using a twin-range cutoff: short-range interactions (within 10 Å) were calculated every time step from a charge-group pair list that was updated every 5 time steps. Long-range forces (up to 15 Å) were determined only every 5 time steps. The Particle-Mesh Ewald (PME) method[28,29] was applied for electrostatic interactions (Ewald parameter $\beta = 3.12$ $nm^{-1}$).

After equilibration, the chosen simulation time was 12 ns for each of the four simulations. The same parameters as in the last step of the equilibration procedure were then adopted throughout.

**2.2. CONCOORD.** The program CONCOORD ("from CONstraints to COORDinates") generates a large number of configurations from a single protein conformation, in a very efficient way.[19] As detailed elsewhere,[19] the method is based on simple distance constraints and a random selection algorithm, thus bypassing costly and lengthy MD simulations involving energetically unfavorable transition states. Here, we used the energy-minimized geometries of the previous section for the dark and the signaling state of the LOV2 domain as generating configurations. From each of the two forms 1000 structures were generated. Water molecules

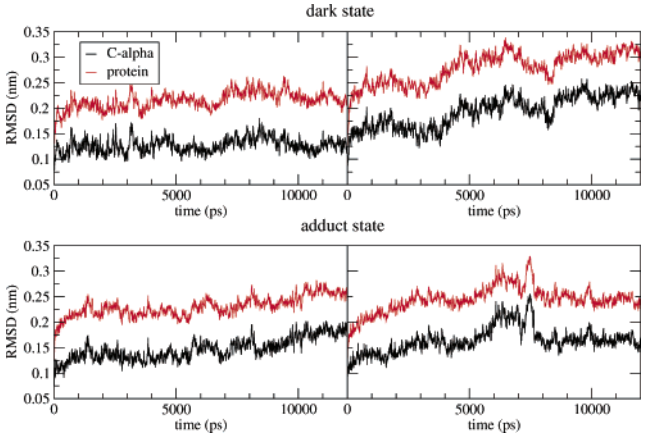


**Figure 2.** Time evolution of RMS deviations with respect to the crystal structures, for the four MD simulations of this work.

(except those present in the crystal structure) and hydrogen atoms were removed before the structures were generated.

## 3. RESULTS AND DISCUSSION

**3.1. Root-Mean-Square Analysis.** In a first step, root-mean-square deviation (RMSD) values were calculated with respect to the crystal structures, for the dark and the illuminated LOV2 domains

$$\mathrm{RMSD}(t) = \sqrt{\frac{1}{M}\sum_{i=1}^{N} m_i |\underline{r}_i(t) - \underline{r}_i^0|^2} \qquad (2)$$

Here, $|\underline{r}_i(t) - \underline{r}_i^0|$ is the actual distance of atom $i$ from its crystal structure position, $N$ is the number of atoms, and $M$ is the total mass which derives from the atom masses, $m_i$. The result is shown in Figure 2 where the RMSD values are given separately for the whole protein and the (104) $C_\alpha$ atoms only. The four panels correspond to the two LOV2 forms, each one treated with two different initial conditions as outlined in section 2.1.

Obviously, the MD simulations lead to stable structures. We find reasonable RMSD values generally for the "all atoms" case (in the range up to 0.25−0.3 nm) and for the $C_\alpha$ atoms in particular (within 0.15−0.25 nm). Both for the dark and the adduct state the second simulation tends to give somewhat larger RMSD values. In addition, the secondary structure of the LOV domains remains intact during the simulations (data not shown).

The flexibility of the backbone can be quantified in more detail by looking at the RMS fluctuations (RMSF), of the $C_\alpha$ atoms

$$\mathrm{RMSF}(i) = \sqrt{\langle \underline{r}_i^2 \rangle - \langle \underline{r}_i \rangle^2} \qquad (3)$$

with $\langle \cdots \rangle$ indicating a time-average. Figure 3 shows the RMSF values for all four simulations. According to these data, the most flexible parts are found within the loops of the protein, as is usual. The RMSF values are especially large around Asn91 and Pro11, both of which reside in the loops connecting the beta-sheets $\beta$D and $\beta$E (Asn91) and $\beta$A and $\beta$B (Pro11), respectively—see Figure 1 for illustration. (The numbering used here starts with 1 at the N-terminal end of the LOV2 domain.) Interestingly, the fluctuation of the $\alpha'$A helix, which directly follows the reactive cysteine residue

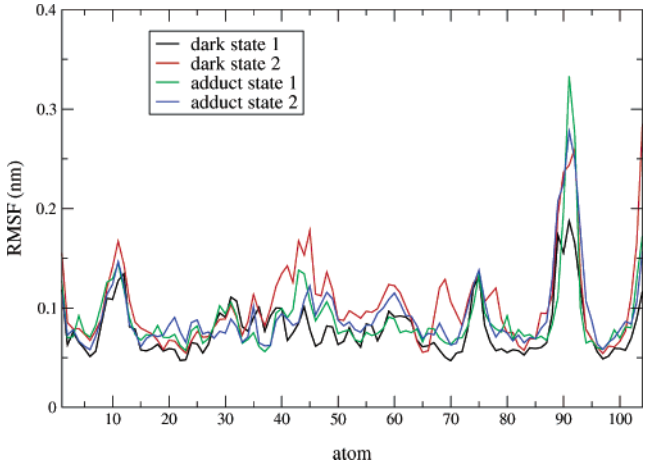


**Figure 3.** RMS fluctuations of the $C_\alpha$ atoms for the MD simulations.

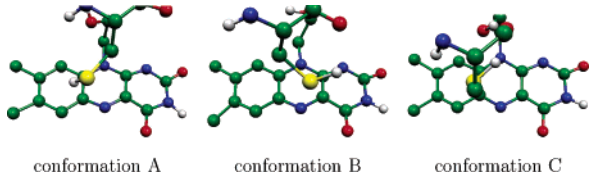


**Figure 4.** Snapshots from the MD simulations showing the three possible conformations of the cysteine residue in the dark state. Red: oxygen; blue: nitrogen; green: carbon; yellow: sulfur; white: hydrogen (not all H's shown).

(Cys38 according to our nomenclature) along the protein backbone, shows a broad variance regarding the RMSF values for the amino acids in that region. Cys38 itself has a reduced flexibility in the adduct state according to the simulations, which is reasonable because then the amino acid is attached to the FMN unit. Other than that, however, there are no clear differences between the dark and illuminated states, within our "error bars". This conclusion is corroborated by the fact that for most parts of the protein the differences in RMSF values arising from different initial conditions are of the same order of magnitude as those due to considering different (dark or illuminated) forms. Most notably, the fluctuations derived from dark state simulation 1 are in general observably lower than those from dark state simulation 2, and the atomic fluctuations of the adduct simulations are between those two extrema. Inspection of RMSF values of all the heavy atoms does not alter this conclusion.

**3.2. Conformations of the Reactive Cysteine Cys38.** While in the dark state crystal structure of the LOV2 domain from *Adiantum capillus-veneris* (resolution: 2.6 Å) only one conformation of the reactive cysteine could be resolved,[16] a more recent, more accurate crystal structure of the LOV1 domain from *Chlamydomonas reinhardtii* (resolution: 1.9 Å) exhibits two different conformers. These are termed conformations A and B in the following and are shown in Figure 4. The conformers originate from a rotation around the $C_\alpha$-$C_\beta$-bond in cysteine. They are found in LOV1 from *Chlamydomonas reinhardtii* with a distribution of approximately 70%:30%.

Both conformations were also seen in our simulations. In addition, a third conformation, C, was found (and expected), see Figure 4. From the MD simulations one can easily extract

**Table 2.** Distribution of the Three Dark State Cysteine Conformers A, B, and C of Figure 4 According to the MD Simulations and the Crystal Structure (of LOV1)[18]

| | dark state sim. 1 (%) | dark state sim. 2 (%) | LOV1[18] (%) |
|---|---|---|---|
| conformation A | 31 | 58 | 70 ± 10 |
| conformation B | 34 | 32 | 30 ± 10 |
| conformation C | 35 | 10 | |

**Table 3.** Mean $\langle R \rangle$ and Standard Deviation $\sigma_R$ of the Distance between the Carboxy C-Atom of Glu32 and the Terminal N-Atom of Lys73 According to the MD Simulations[a]

| | dark state | | | adduct state | | |
|---|---|---|---|---|---|---|
| | sim. 1 | sim. 2 | LOV2 | sim. 1 | sim. 2 | LOV2 |
| $\langle R \rangle$ [Å] | 4.28 | 3.93 | 3.20 | 4.06 | 4.15 | 3.23 |
| $\sigma_R$ [Å] | 1.20 | 0.72 | | 1.06 | 1.10 | |

[a] For comparison, the LOV2 crystal structure data are also given.[16,17]

the (time-averaged) probabilities according to which the various conformers A, B, and C occur, in the dark state of LOV2 from *Adiantum capillus-veneris*. According to Table 2, in simulation 1 the three conformers are populated with about equal probability, whereas simulation 2 (with different initial conditions) reproduces the experimental findings (for LOV1 from *Chlamydomonas reinhardtii*, though), more closely. Further analysis reveals that conformations A and B isomerize to each other on a ps time scale; in contrast, conformation C is—once reached—stable for rather long times (ns time scale). In fact, the fractions of conformation C in Table 2 arise from a *single* time window in each of the two simulations, in which only conformation C is found. Therefore, the statistics particularly for simulation 1 is biased somewhat, and the MD simulation appears to be quite compatible with the experimental crystal structure. In general, the existence of two or three conformations of the reactive cysteine residue may explain the experimental observation of an at least biexponential kinetics for the adduct formation.[11]

**3.3. Stability of the Salt Bridge Glu32-Lys73.** According to a recent proposal by Crosson et al., adduct formation in the LOV domain leads to a reduced stability of a Glu-Lys salt bridge on the surface of the LOV domain.[1] The salt bridge, consisting of Glu32 and Lys73, is indicated in Figure 1. To address this hypothesis on the basis of MD simulations, we computed (i) the mean distance, $\langle R \rangle$, between the carboxy C-atom of Glu32 and the terminal N-atom of Lys73 and (ii) the variance, $\sigma_R$, of this distance in the dark and in the adduct state simulations. In particular, $\sigma_R$ serves as a measure for the flexibility of the salt bridge, while the $\langle R \rangle$ are less conclusive for dynamics. The results are summarized in Table 3. Again, it is not possible to prove a clear trend regarding the dark and illuminated state of the LOV domain, based on our MD simulations. Within our error bars, the flexibility of the salt bridge appears to be unaffected when going from the dark to the illuminated state. In comparison to experiment, however, our mean distances $\langle R \rangle$ are significantly larger, with the possible implication that the salt bridge is less stable in water solution than in the crystals which were used for diffraction.

**3.4. Principal Component Analysis.** Finally, a principal component analysis (also named essential dynamics analysis)

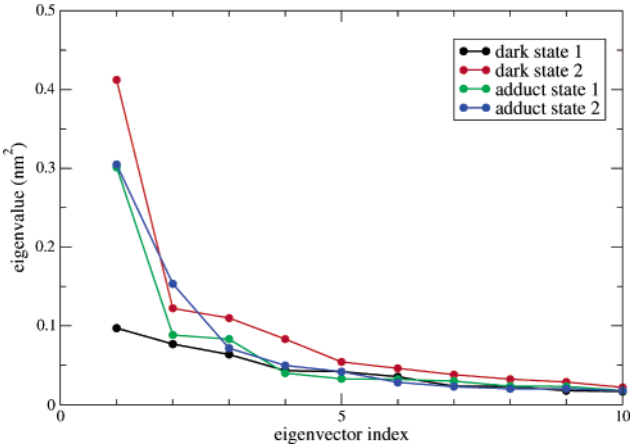


**Figure 5.** The largest 10 eigenvalues of the covariance matrix from the MD simulations.

was carried out. To do this, the covariance matrix, defined by

$$C_{ij} = \langle (x_i - \langle x_i \rangle)(x_j - \langle x_j \rangle) \rangle \quad (4)$$

has to be computed and diagonalized. Here, $x_i(t)$ is the trajectory of atom $i$ along Cartesian coordinate $x$, and $\langle x_i \rangle$ is the corresonding average value. The covariance matrix is symmetric and of size $3N \times 3N$. The eigenvectors $\underline{a}_i$ of this matrix are related to the coupled modes of the protein. The eigenvalue for a particular mode gives the corresponding variance, which again is a useful measure for the "mobility" of that mode.[30,31] Therefore, those eigenvectors with the largest eigenvalues correspond to the principal motions of the protein. In our analysis, only the $C_\alpha$ atoms were used as a basis (resulting in a matrix of size 312 × 312), which is sensible in view of the finding that including more atoms does not change the results significantly.[30]

Figure 5 shows the computed eigenvalues for all MD simulations. Except for the first dark state simulation, we find that the eigenvalue distribution is clearly dominated by the first few eigenvalues only. In case of dark state simulation 1, however, the distribution of eigenvalues is somewhat more flat. A comparison of the eigenvalues between the different simulations indicates the same phenomenon as already mentioned in the discussion of the RMSF values: obviously dark state simuation 1 leads to the least flexible trajectory, while dark state simulation 2 gives the most flexible one, the adduct state simulations lying somewhere in between. We also carried out the principal component analysis for different parts of the protein, but the results did not change qualitatively, essentially resembling the results already derived from the RMSF and PCA calculations.

In Figure 6 the atomic displacements according to the eight most important eigenvectors (with the largest eigenvalues) are compared, for all four MD runs of this work. The atomic displacement of atom $k$ is given by

$$\mathrm{disp}_i(k) = |\underline{a}_i^{(k)}| \quad (5)$$

with $\underline{a}_i^{(k)}$ being the subvector of $\underline{a}_i$ which contains the x-, y-, and z-component corresponding to atom $k$. Similar to the conclusions drawn from the RMSD values in Figure 2, we note that the most flexible parts of the protein are around Pro11, Asn91, and in the region around Cys38. While Figure

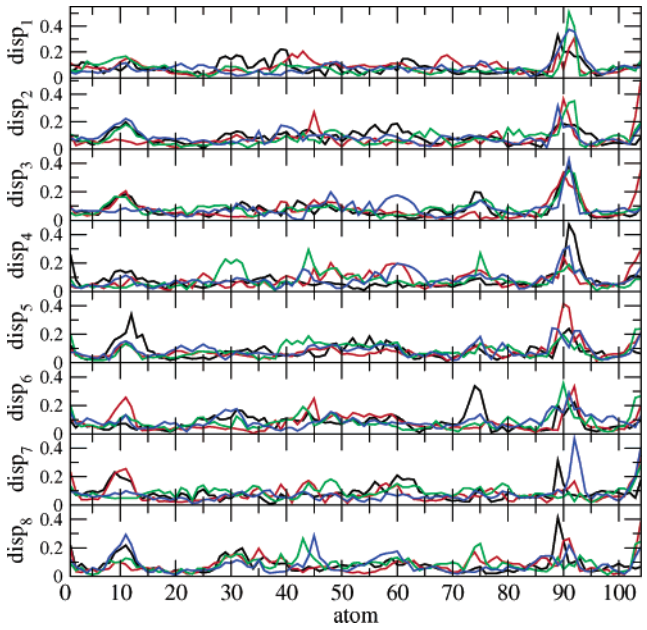


**Figure 6.** Atomic displacements in nm according to the eight most important eigenvectors from the principal value analysis of the MD simulations. Coloring is as in Figure 5.

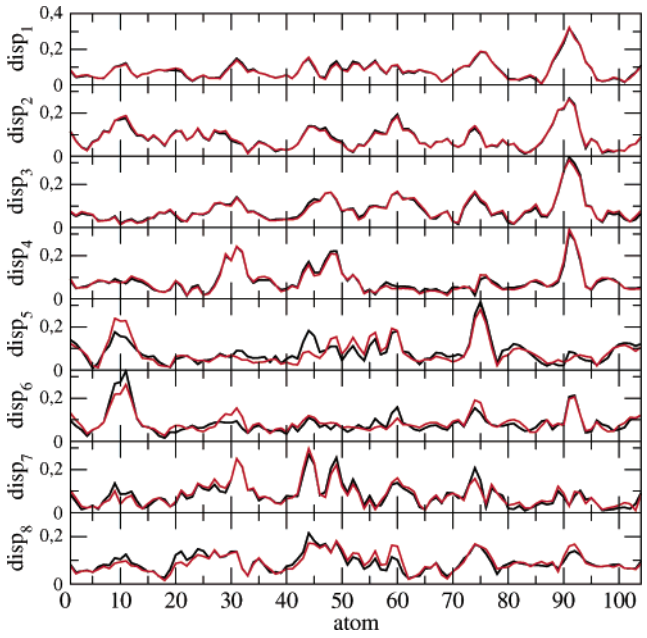


**Figure 7.** Atomic displacements in nm according to the eight most important eigenvectors from the principal value analysis of the CONCOORD simulations. Black: dark state; red: illuminated state.

6 gives a more detailed, i.e. mode-resolved, insight into the flexibility of the protein, the sampling is again not good enough even after 12 ns to unambiguously detect significant differences between the dark and the adduct state of the LOV domain.

To improve on that and thus to allow for a better sampling, the CONCOORD method[19] described in section 2.1 was used as an additional tool. The eigenvectors of the covariance matrix which were obtained from the CONCOORD ensembles are shown, for the dark and the adduct form, in Figure 7. From the figure we note that both forms are extremely similar in their eigenvectors $\underline{a}_1$-$\underline{a}_4$, which exhibit the largest eigenvalues, and still quite similar for eigenvectors $\underline{a}_6$-$\underline{a}_8$. The biggest differences between the dark and the illuminated forms are for eigenvector $\underline{a}_5$, in particular around amino acid Arg44. Arg44 is located between the α′A and αC motifs of Figure 1 and seems to be somewhat more flexible in the dark state. However, it is again found that the differences are too small to be conclusive. Also, only small distinctive features are visible at and around the salt bridge (small effects for Glu32, none for Lys73, small effects in their neighborhoods).

## 4. CONCLUSIONS

In summary, based on MD simulations and the CONCOORD method no clear changes in the structure or in the dynamics, relevant for signal transduction, could be established upon adduct formation within the LOV2 domain from *Adiantum capillus-veneris*. Also, the hypothesis of the reduced stability of the Glu-Lys salt bridge on the surface of the LOV domain finds no support by the simulations.

We therefore support the hypothesis that the available crystal structures do not contain all information necessary to understand the signaling process. One may speculate that the structures of the LOV domains are somewhat distorted by crystallization. It seems more likely, however, that an essential part of the protein which interacts with the LOV domains is missing in the available crystal structures. Very recent NMR experiments with C-terminally elongated LOV domains by Harper et al. hint to this possibility.[32] There is an amphiphatic α helix following the *β*E strand (Figure 1), which not only takes two different orientations toward the rest of the LOV domain in the two states but also has a critical effect on the conformation of the PAS core in the dark state. Taken together, the crystal structures show only the conformation of the PAS core without that interaction, which is possibly why the MD simulations based on these structures do not account for any significant differences between dark and illuminated states of the LOV domain. Unfortunately, the NMR data led only a low-resolution structure not suitable for MD simulations. Especially the dark state structure with the adjoining α-helix would be interesting to model, since this structure seems to be clearly distorted (according to the chemical shifts measured by NMR) from the structures without that helix which were studied here.

Apart from suggesting further experimental and theoretical work along these directions, the present MD simulations offer already some interesting insight into details of the photochemistry and photophysics of LOV domains. One such detail is the occurrence of different conformations A, B (and C) in the adduct state and the time scales for their interconversion.

## ACKNOWLEDGMENT

This work was supported by the Deutsche Forschungsgemeinschaft (DFG), within the *Graduiertenkolleg* "*Sensory photoreceptors in natural and artificial systems*" (GK640/1).

**Supporting Information Available:** The parametrization along with a pictorial representation of "cysteinyl-FMN". This material is available free of charge via the Internet at http://pubs.acs.org.

## REFERENCES AND NOTES

(1) Crosson, S.; Rajagopal, S.; Moffat, K. The LOV Domain Family: Photoresponsive Signaling Modules Coupled to Diverse Output Domains. *Biochemistry* **2003**, *42*, 2−10.

(2) Huala, E. P.; Oeller, P. W.; Liscum, E.; Han, I.-S.; Larsen, E.; Briggs, W. R. *Arabidopsis* NPH1: A Protein Kinase with a Putative Redox-Sensing Domain. *Science* **1997**, *278*, 2120−2130.
(3) Christie, J. M.; Reymond, P.; Powell, G. K.; Bernasconi, P.; Raibekas, A. A.; Liscum, E.; Briggs, W. R. *Arabidopsis* NPH1: A Flavoprotein with the Properties of a Photoreceptor for Phototropism. *Science* **1998**, *282*, 1698−1701.
(4) Jarillo, J. A.; Gabrys, H.; Capel, J.; Alonso, J. M.; Ecker, J. R.; Cashmore, A. R. Phototropin-Related NPL1 Controls Chloroplast Relocation Induced by Blue Light. *Nature* **2001**, *410*, 952−954.
(5) Kagawa, T.; Sakai, T.; Suetsugu, N.; Oikawa, K.; Ishiguro, S.; Kato, T.; Tabata, S.; Okada, K.; Wada, M. *Arabidopsis* NPL1: A Phototropin Homologue Controlling the Chloroplast High-Light Avoidance Response. *Science* **2001**, *291*, 2138−2141.
(6) Kinoshita, T.; Doi, M.; Suetsugu, N.; Kagawa, T.; Wada, M.; Shimazaki, K. I. Phot1 and Phot2 Mediate Blue Light Regulation of Stomatal Opening. *Nature* **2001**, *414*, 656−660.
(7) Huang, K.; Beck, C. F. Isolation and charcterization of a *Chlamydomonas* gene that encodes a blue-light photoreceptor of the phototropin family. In *Tenth International Conference on the Cell and Molecular Biology of Chlamydomonas reinhardtii*; University of Vancouver, British Columbia, 2002.
(8) Huang, K.; Merkle, T.; Beck, C. F. Isolation and charcterization of a *Chlamydomonas* gene that encodes a putative blue-light photoreceptor of the phototropin family. *Physiol. Plant* **2002**, *115*, 613−622.
(9) Christie, J. M.; Swartz, T. E.; Bogomolni, R. A.; Briggs, W. R. Phototropin LOV domains exhibit distinct roles in regulating photoreceptor function. *Plant J.* **2002**, *32*, 205−219.
(10) Ataka, K.; Hegemann, P.; Heberle, J. Vibrational Spectroscopy of an Algal Phot-LOV1 Domain Probes the Molecular changes Associated with Blue-Light Reception. *Biophys. J.* **2003**, *84*, 466−474.
(11) Kottke, T.; Heberle, J.; Hehn, D.; Dick, B.; Hegemann, P. Phot-LOV1: Photocycle of a Blue-Light Receptor Domain from the Green Alga *Chlamydomonas reinhardtii*. *Biophys. J.* **2003**, *84*, 1192−1201.
(12) Schüttrigkeit, T. A.; Kompa, C. K.; Salomon, M.; Rüdiger, W.; Michel-Beyerle, M. E. Primary Photophysics of the FMN Binding LOV2 domain of the Plant Blue Light Receptor Phototropin of *Avena sativa*. *Chem. Phys.* **2003**, *294*, 501−508.
(13) Neiss, C.; Saalfrank, P. Ab Initio Quantum Chemical Investigation of the First Steps of the Photocycle of Phototropin: A Model Study. *Photochem. Photobiol.* **2003**, *77*, 101−109.
(14) Salomon, M.; Christie, J. M.; Knieb, E.; Lempert, U.; Briggs, W. R. Photochemical and Mutational Analysis of the FMN−Binding Domains of the Plant Blue Light Receptor, Phototropin. *Biochemistry* **2000**, *39*, 9401−9410.
(15) Swartz, T. E.; Corchnoy, S. B.; Christie, J. M.; Lewis, J. W.; Szundi, I.; Briggs, W. R.; Bogomolni, R. A. The Photocycle of a Flavin-Binding Domain of the Blue Light Photoceptor Phototropin. *J. Biol. Chem.* **2001**, *276*, 36493−36500.
(16) Crosson, S.; Moffat, K. Structure of a Flavin-Binding Plant Photoreceptor Domain: Insights into Light-Mediated Signal Transduction. *Proc. Natl. Acad. Sci. U.S.A.* **2001**, *98*, 2995−3000.
(17) Crosson, S.; Moffat, K. Photoexcited structure of a Plant Photoreceptor Domain Reveals a Light-Driven Molecular Switch. *Plant Cell* **2002**, *14*, 1067−1075.
(18) Fedorov, R.; Schlichting, I.; Hartmann, E.; Domratcheva, T.; Fuhrmann, M.; Hegemann, P. Crystal Structures and Molecular Mechanism of a Light-Induced Signaling Switch: The Phot-LOV1 Domain from *Chlamydomonas reinhardtii*. *Biophys. J.* **2003**, *84*, 2474−2482.
(19) de Groot, B. L.; van Aalten, D. M. F.; Scheek, R. M.; Amadei, A.; Vriend, G.; Berendsen, H. J. C. Prediction of Protein Conformational Freedom from Distance Constraints. *Proteins: Struct. Funct. Gen.* **1997**, *29*, 240−251.
(20) Lindahl, E.; Hess, B.; van der Spoel, D. GROMACS 3.0: A Package for Molecular Simulation and Trajectory Analysis. *J. Mol. Mod.* **2001**, *7*, 306−317.
(21) Berendsen, H. J. C.; van der Spoel, D.; van Drunen, R. GROMACS: A Message-Passing Parallel Molecular Dynamics Implementation. *Comput. Phys. Comm.* **1995**, *91*, 43−56.
(22) van Gunsteren, W. F.; Billeter, S. R.; Eising, A. A.; Hünenberger, P. H.; Krüger, P.; Mark, A. E.; Scott, W. R. P.; Tironi, I. G. *Biomolecular Simulation: The GROMOS96 Manual and User Guide;* Hochschulverlag AG an der ETH Zürich: Zürich, Switzerland, 1996.
(23) Humphrey, W.; Dalke, A.; Schulten, K. VMD − Visual Molecular Dynamics. *J. Mol. Graphics* **1996**, *14.1*, 33−38.
(24) Berendsen, H. J. C.; Postma, J. P. M.; van Gunsteren, W. F.; Hermans, J. Interaction Models for Water in Relation to Protein Hydration. In *Intermolecular Forces*; Pullman, B., Ed.; Reidel: Dordrecht, The Netherlands, 1981.
(25) Berendsen, H. J. C.; Postma, J. P. M.; DiNola, A.; Haak, J. R. Molecular Dynamics with Coupling to an External Bath. *J. Chem. Phys.* **1984**, *81*, 3684−3690.
(26) Miyamoto, S.; Kollman, P. A. SETTLE: An Analytical Version of the SHAKE and RATTLE Algorithm for Rigid Water Molecules. *J. Comput. Chem.* **1992**, *13*, 952−962.
(27) Hess, B.; Bekker, H.; Berendsen, H. J. C.; Fraaije, J. G. E. M. LINCS: A Linear Constraint Solver for Molecular Simulations. *J. Comput. Chem.* **1997**, *18*, 1463−1472.
(28) Darden, T.; York, D.; Pedersen, L. Particle Mesh Ewald: An $N\cdot\log(N)$ Method for Ewald Sums in Large Systems. *J. Chem. Phys.* **1993**, *98*, 10089−10092.
(29) Essmann, U.; Perera, L.; Berkowitz, M. L.; Darden, T.; Lee, H.; Pedersen, L. G. A Smooth Particle Mesh Ewald Method. *J. Chem. Phys.* **1995**, *103*, 8577−8593.
(30) Amadei, A.; Linssen, A. B. M.; Berendsen, H. J. C. Essential Dynamics of Proteins. *Proteins: Struct. Funct. Gen.* **1993**, *17*, 412−425.
(31) Kitao, A.; Go, N. Investigating Protein Dynamics in Collective Coordinate Space. *Curr. Op. Struct. Biol.* **1999**, *9*, 164−169.
(32) Harper, S. M.; Neil, L. C.; Gardner, K. H. Structural Basis of a Phototropin Light Switch. *Science* **2003**, *301*, 1541−1544.

CI049883U